The SWELLS survey

Dutton, Aaron A.; Treu, Tommaso; Brewer, Brendon J.; Marshall, Philip J.; Auger, M. W.; Barnabe, Matteo; Koo, David C.; Bolton, Adam S.; Koopmans, Leon V. E.

Published in:
Monthly Notices of the Royal Astronomical Society

DOI:
10.1093/mnras/sts262

Monthly Notices
of the
ROYAL ASTRONOMICAL SOCIETY

MNRAS **428,** 3183–3195 (2013) doi:10.1093/mnras/sts262

The SWELLS survey – V. A Salpeter stellar initial mass function in the bulges of massive spiral galaxies

Aaron A. Dutton,[1,2]★ Tommaso Treu,[2]† Brendon J. Brewer,[2,3] Philip J. Marshall,[4] M. W. Auger,[2,5] Matteo Barnabè,[6] David C. Koo,[7] Adam S. Bolton[8] and Leon V. E. Koopmans[9]

[1]*Max Planck Institute for Astronomy, Königstuhl 17, D-69117 Heidelberg, Germany*
[2]*Department of Physics, University of California, Santa Barbara, CA 93106, USA*
[3]*Department of Statistics, The University of Auckland, Private Bag 92019, Auckland 1142, New Zealand*
[4]*Department of Physics, University of Oxford, Keble Road, Oxford OX1 3RH*
[5]*Institute of Astronomy, University of Cambridge, Madingley Rd, Cambridge CB3 0HA*
[6]*Kavli Institute for Particle Astrophysics and Cosmology, Stanford University, 452 Lomita Mall, Stanford, CA 94035, USA*
[7]*UCO/Lick Observatory, Department of Astronomy and Astrophysics, University of California, Santa Cruz, CA 95064, USA*
[8]*Department of Physics and Astronomy, University of Utah, Salt Lake City, UT 84112, USA*
[9]*Kapteyn Astronomical Institute, University of Groningen, PO Box 800, NL-9700 AV Groningen, the Netherlands*

Accepted 2012 October 22. Received 2012 October 12; in original form 2012 June 19

ABSTRACT

Recent work has suggested that the stellar initial mass function (IMF) is not universal, but rather is correlated with galaxy stellar mass, stellar velocity dispersion or morphological type. In this paper, we investigate variations of the IMF within individual galaxies. For this purpose, we use strong lensing and gas kinematics to measure independently the normalization of the IMF of the bulge and disc components of a sample of five massive spiral galaxies with substantial bulge components taken from the Sloan WFC Edge-on Late-type Lens Survey (SWELLS). We find that the stellar masses of the bulges are tightly constrained by the lensing and kinematic data. A comparison with masses based on stellar population synthesis models fitted to optical and near-infrared photometry favours a Salpeter-like normalization of the IMF. Conversely, the disc masses are less well constrained due to degeneracies with the dark matter halo, but are consistent with Milky Way-type IMFs in agreement with previous studies. The discs are submaximal at 2.2 disc scale lengths, but due to the contribution of the bulges, the galaxies are baryon dominated at 2.2 disc scale lengths. Globally, our inferred IMF normalization is consistent with that found for early-type galaxies of comparable stellar mass ($>10^{11}\,M_{\odot}$). Our results suggest a non-universal IMF within the different components of spiral galaxies, adding to the well-known differences in stellar populations between discs and bulges.

Key words: stars: luminosity function, mass function – galaxies: bulges – galaxies: kinematics and dynamics – galaxies: spiral – dark matter.

1 INTRODUCTION

The stellar initial mass function (IMF) is a fundamental quantity in many areas of astrophysics. From a theoretical standpoint, understanding the origin of the IMF from first principles is essential to develop a complete theory of star formation (e.g. McKee & Ostriker 2007). From a phenomenological standpoint, the IMF is a defining property of any stellar population, essential for computing quantities such as stellar mass from observables and for characterizing their evolutionary history.

Traditionally, the main source of empirical evidence regarding the stellar IMF has been our own Milky Way, where individual stars can be identified and counted, first by Salpeter (1955). In the decades since then, only relatively small variations of the IMF have been found within our own Milky Way, despite enormous variations in the physical conditions within star-forming regions. These results have been generally interpreted as evidence that the IMF is more or less universal – i.e. it is insensitive to the properties of the gas and dust in which stars form (e.g. Bastian, Covey & Meyer 2010). If indeed the IMF is universal, the kinematics of spiral (Bell & de

★ E-mail: dutton@mpia.de
†Packard Research Fellow.

Jong 2001) and elliptical galaxies (Cappellari et al. 2006), as well as lensing data (Brewer et al. 2012, hereafter SWELLS-III), rule out IMFs like Salpeter's implying relatively 'heavy' mass-to-light ratios, in favour of 'lighter' IMFs like those measured by Kroupa (2001) and Chabrier (2003).

However, recently a number of independent extragalactic studies have found significant deviations from the IMF as measured in the Milky Way. The observations are based on a variety of independent techniques, ranging from gravitational lensing (Auger et al. 2010; Treu et al. 2010; Spiniello et al. 2011; Brewer et al. 2012) to stellar kinematics of elliptical galaxies (e.g. Cappellari et al. 2012a; Dutton, Mendel & Simard 2012a; Dutton et al. 2012b), and to spectral diagnostics of stellar populations (van Dokkum & Conroy 2010, 2011; Conroy & van Dokkum 2012; Spiniello et al. 2012).

Based on these observations, it appears that the IMF may depend on the stellar mass of the galaxy and hence on the cosmological time at which the stars formed, possibly reflecting the evolving physical conditions in the expanding universe. Or perhaps it could depend on the stellar velocity dispersion, reflecting the depth of the potential well. It is also possible that the IMF might depend on the morphological type of the galaxy, in the sense that early-type galaxies (ETGs) might have 'heavier' IMFs than their spiral counterparts. However, the dependence of the distribution of morphological types on stellar mass (e.g. Blanton & Moustakas 2009), as well as the presence of two very distinct stellar populations in the bulges and discs of typical galaxies (e.g. Wyse, Gilmore & Franx 1997), makes it unclear whether the more important parameter is the overall stellar mass, or stellar velocity dispersion or the morphological type.

In this paper we aim to gather some insight into the physical origin of the non-universality of the IMF by looking for variations *within* individual spiral galaxies. Is the normalization of the IMF the same for bulge and disc, just varying with total stellar mass? Or is there one universal normalization for disc-like stellar populations (presumably Chabrier-like) and a 'heavier' (Salpeter-like) one for the older and more metal-rich stellar populations found in massive bulges and spheroids? Clearly, the two hypotheses are not mutually exclusive, as a combination of both could be at play.

Our strategy to constrain the IMF normalization consists of comparing stellar masses derived from dynamics and strong lensing to those derived from stellar population synthesis (SPS) models. The main challenge of this approach – and of all other dynamical approaches – is that lensing and dynamics are sensitive to the total mass, and therefore one needs to disentangle the stellar mass from the non-baryonic dark matter. For disc-dominated galaxies it is well known that rotation curves can be fitted with a wide range of stellar mass-to-light ratios, from zero to maximum disc (e.g. van Albada & Sancisi 1986; Dutton et al. 2005), the so-called disc–halo degeneracy (see however Amorisco & Bertin 2010). For bulge-dominated systems, the situation is similar in principle (the so-called bulge–halo degeneracy). However, if the stellar mass of the bulge dominates the inner parts of the gravitational potential, it is possible to get an actual measurement (rather than an upper limit), with only modest assumptions about the density profile of the dark matter halo, e.g. inspired by the results of cosmological numerical simulations (Treu & Koopmans 2002; Koopmans & Treu 2003; Auger et al. 2010; Treu et al. 2010; Cappellari et al. 2012a; see also Bertin et al. 1994, and references therein).

In order to study the IMF of the bulge and disc components, we apply the lensing and dynamical technique to the sample of five massive ($V_{2.2} \sim 250$–$300\,\mathrm{km\,s^{-1}}$, $M_{\rm SPS}^{\rm Chab} \sim 10^{11}\,\mathrm{M_\odot}$) spiral lens galaxies in the SWELLS Survey (Treu et al. 2011, hereafter SWELLS-I) with significant bulges (bulge-to-disc ratio $\gtrsim$0.5 assuming a universal IMF) and for which ionized gas kinematic data are available. SWELLS is a dedicated survey to the study of lensing spiral disc galaxies. Its main properties are summarized in Section 2. More details can be found in the paper by Treu et al. (2011). Thus, our mass models are constrained by the projected mass within the Einstein radius measured by strong gravitational lensing, by the rotation curve of the outer disc ∼1–3 scale lengths from ionized gas kinematics, and the high-resolution surface brightness profiles which are decomposed into a de Vaucouleurs bulge and an exponential disc. We derive stellar masses of the bulge and disc for a variety of assumptions about the structure of the dark matter halo, and compare the results with the estimates from SPS models to infer the normalization of the IMF independently for the two components.

This paper is organized as follows. In Section 2 we present the observational constraints. In Section 3 we present the mass models. In Section 4 we present our main results. In Section 5 we discuss possible sources of systematic errors. In Section 6 we conclude with a brief summary. Throughout, we assume a flat Λ cold dark matter (ΛCDM) cosmology with present-day matter density $\Omega_{\rm m} = 0.3$ and Hubble parameter $H_0 = 70\,\mathrm{km\,s^{-1}\,Mpc^{-1}}$.

2 SAMPLE SELECTION AND DATA

In this section we describe the sample selection and give a brief description of the data used in this paper. The reader is referred to papers SWELLS-I, SWELLS-II (Dutton et al. 2011b), SWELLS-III and SWELLS-VI (Dutton et al., in preparation) for more details on the SWELLS selection and data.

2.1 Sample selection

As detailed in paper I, the parent SWELLS sample is selected from the Sloan Digital Sky Survey (SDSS) spectroscopic data base based on detecting emission lines at multiple redshifts within the 3 arcsec fibre and on having a photometric axis ratio of <0.6. Multiband *Hubble Space Telescope* (*HST*) imaging is used to confirm the lensing hypothesis. The sample of 20 confirmed lenses spans a broad range of bulge to total stellar mass ratio (from 0.1 to 0.9) for a fixed universal IMF, and a range in stellar mass of over one decade ($\sim 10^{10}$ to $10^{11.5}\,\mathrm{M_\odot}$; for a Chabrier IMF).

An important question is whether the SWELLS sample is representative of the overall population of spiral galaxies within the same ellipticity and stellar mass limits. Paper I shows that the size–stellar mass relation of the SWELLS sample is indistinguishable from that of a control sample of SDSS-selected galaxies using the same criteria. Paper VI will investigate the selection function in more detail using kinematic data to construct the Tully–Fisher, Faber–Jackson and Fundamental Plane correlations.

The subsample analysed in this paper is selected from the SWELLS survey to include all the massive spiral galaxies with significant bulges for which gas-kinematic rotation curves are available. We require the stellar mass in the disc to be less than two times the stellar mass in the bulge, a criterion that is met by all but two of the lenses in our sample (we also exclude one system that has been shown to have a pseudo-bulge) although only five of these systems also have gas rotation curves available. A montage of our selected subsample of galaxies is shown in Fig. 1. The subsample includes some (but not all) of the most massive SWELLS lenses. Quantitatively, the subsample spans a range in lensing velocity dispersion of 196–251 $\mathrm{km\,s^{-1}}$, i.e. galaxies that are more massive than our own Milky Way, and spanning the 230 $\mathrm{km\,s^{-1}}$ threshold below which

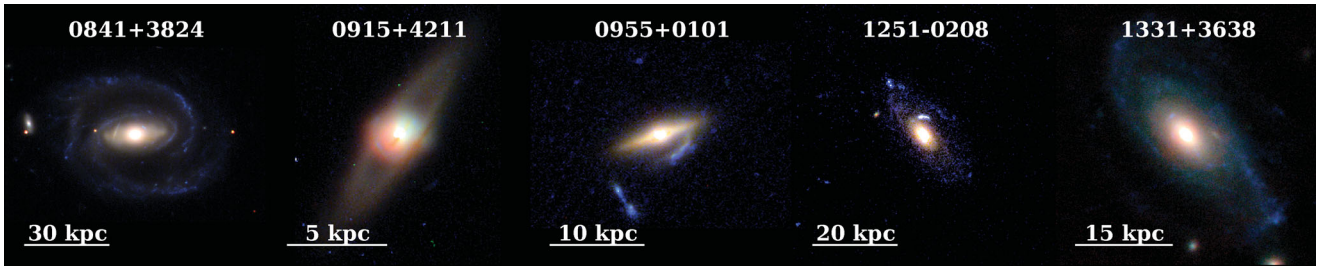

Figure 1. Postage stamp images of the galaxies analysed in this paper. The images are obtained from multicolour *HST* images as described in SWELLS-I and III.

Table 1. Basic properties of galaxies analysed in this paper. All errors correspond to 1σ. Column 1 lists the lens ID; Column 2 the redshift of the deflector; Column 3 gives the velocity dispersion of the singular isothermal ellipsoid (SIE) lens model from paper III; Columns 4 and 5 give half-light sizes for the bulge (circularized) and disc (major axis) from papers I and III; Columns 6, 7 and 8 give the stellar masses for the bulge, disc and total, assuming a Chabrier (2003) IMF; Columns 9 and 10 give the model (dust-reddened) rest-frame V-band luminosities for the bulge and disc; Columns 11 and 12 give the model $(B-V)$ colours for the bulge and disc.

ID	$z_{\rm d}$	$\sigma_{\rm SIE}$ (km s^{-1})	$R_{\rm bulge}$ (kpc)	$R_{\rm disc}$ (kpc)	$\log(M^{\rm Chab}_{\rm SPS,b})$ ($M_\odot$)	$\log(M^{\rm Chab}_{\rm SPS,d})$ ($M_\odot$)	$\log(M^{\rm Chab}_{\rm SPS,t})$ ($M_\odot$)	$\log(L_{V,\rm b})$ ($L_{\odot,V}$)	$\log(L_{V,\rm d})$ ($L_{\odot,V}$)	$(B-V)_{\rm b}$	$(B-V)_{\rm d}$
(1)	(2)	(3)	(4)	(5)	(6)	(7)	(8)	(9)	(10)	(11)	(12)
J0841+3824	0.116	251.2 ± 4.4	2.42	23.43	11.05 ± 0.09	11.23 ± 0.09	11.45 ± 0.07	10.54 ± 0.04	10.84 ± 0.04	0.79	0.70
J0915+4211	0.078	195.7 ± 2.2	1.56	4.15	10.60 ± 0.09	10.17 ± 0.09	10.74 ± 0.08	10.03 ± 0.05	9.73 ± 0.05	0.81	0.72
J0955+0101	0.111	238.4 ± 7.3	1.62	3.72	10.63 ± 0.09	10.17 ± 0.09	10.76 ± 0.07	10.00 ± 0.04	9.73 ± 0.04	0.87	0.73
J1251−0208	0.224	203.0 ± 2.6	1.68	12.01	10.68 ± 0.07	10.96 ± 0.07	11.14 ± 0.06	10.16 ± 0.04	10.68 ± 0.03	0.82	0.65
J1331+3638	0.113	248.1 ± 4.4	2.86	12.46	10.89 ± 0.10	10.46 ± 0.10	11.03 ± 0.07	10.38 ± 0.04	10.34 ± 0.04	0.78	0.47

paper III concluded that a global Salpeter IMF is on average ruled out by the data. Basic properties of the subsample analysed in this paper are given in Table 1.

2.2 Strong lensing

Strong lensing models for our sample galaxies are presented in SWELLS-III. The parameter that is most directly constrained by strong lensing is the circularized Einstein radius b (Treu 2010, and references therein). This is defined to be the radius inside which the average surface density is equal to the critical density for strong lensing:

$$\frac{M_{\rm proj}(b)}{\pi b^2} = \Sigma_{\rm crit} \equiv \frac{c^2}{4\pi G}\frac{D_{\rm s}}{D_{\rm ds}D_{\rm d}}. \quad (1)$$

Here $D_{\rm s}$ is the angular diameter distance from the observer to the source, $D_{\rm d}$ is the angular diameter distance from the observer to the deflector (i.e. the lens) and $D_{\rm ds}$ is the angular diameter distance from the deflector to the source. The critical density thus depends only on the distances to the lens and source, which are known for all our lens systems from the SDSS redshifts and our adopted cosmology.

For comparison to kinematics it is convenient to express the lensing results in terms of circular velocity or velocity dispersion, where $V_{\rm SIE} = \sqrt{2}\sigma_{\rm SIE}$. However, since the mass profiles are in general not isothermal, the conversion from projected mass into circular velocity at the Einstein radius is non-trivial. For a total mass profile steeper than isothermal, which is the case for our galaxies, the circular velocity at the Einstein radius is larger than the nominal circular velocity of the singular isothermal ellipsoid (SIE) model.

Thus, in our mass models in this paper we fit directly for b, rather than the mass projected within b [due to covariance between $M_{\rm proj}(b)$ and b], or the derived circular velocity/velocity dispersion at the Einstein radius.

2.3 Gas kinematics

We obtained major axis long-slit spectra for all five galaxies with the Low Resolution Imaging Spectrograph (Oke et al. 1995) on the Keck I 10-m telescope between 2008 November and 2011 April. Typical exposure times were 60 min, with seeing conditions of full width at half-maximum (FWHM) $\sim$ 1.0 arcsec. On the red side we used the 600/7500 line grating which gives a pixel scale of 1.26 Å pixel^{-1}. With a 1 arcsec wide slit the resulting spectral resolution is $\simeq$ 4.2 Å, corresponding to a velocity dispersion resolution of $\sim$70 km s^{-1} at the wavelength of Hα. We adopt spatial samplings of $\simeq$ 1.1–1.5 arcsec (5–7 pixels) corresponding to $\sim$1 data point per seeing FWHM.

We measured rotation curves by fitting Gaussians to one-dimensional spectra extracted along the slit. To improve centroiding accuracy we fitted the redshift of neighbouring emission lines simultaneously. The primary set of emission lines are Hα 6563, [N II] 6583, 6548. The line flux ratios between the two [N II] lines were fixed at the expected values. The velocity dispersions of the line pairs were also imposed to be the same, but were allowed to be different than Hα. The continuum was fitted with a second-order polynomial.

The observed rotation velocities are lowered from the true circular velocities by several effects. First, there is a $\sin(i)$ term due to the inclination, i, of the galaxy with respect to the line of sight. Secondly, there is the (potential) position angle offset of the slit from the kinematic major axis. Thirdly, there is beam smearing due to finite slit width and seeing. These effects are taken into account in our modelling. We create model velocity fields and extract flux-weighted rotation velocities inside a 1 arcsec wide slit, which has a position angle offset from the major axis. For this calculation we assume that the line-emitting gas traces the stellar disc. This assumption is the major source of systematic uncertainty in our models. To minimize the impact of the uncertainties in the beam

smearing model, we exclude from our fits the inner few arcseconds of the kinematic data. We also exclude data points where the rotation curve is strongly asymmetric (such as due to the bar in J0841+3824) or where the signal-to-noise ratio is low (such as in interspiral arm regions). We treat the disc inclination angle and slit position angle offsets as nuisance parameters, allowing them to vary over suitably chosen small ranges. We determine that an initial guess for the inclination from the disc minor-to-major axis ratio $q_{\rm d}$ assuming $\cos(i) = \sqrt{(q_{\rm d}^2 - q_0^2)/(1 - q_0^2)}$, where $q_0 \simeq 0.2$ (e.g. Hall et al. 2012) is the intrinsic disc thickness.

2.4 Bulge and disc structural parameters

The light profiles are decomposed into bulges and discs as described in papers SWELLS-I and III. The bulge light profile is assumed to follow a Sérsic $n = 4$ (de Vaucouleurs) profile, while the disc profile is assumed to be Sérsic $n = 1$ (exponential) profile. We note that 0841+3824 is a barred spiral galaxy. However, the bar is significantly fainter than the bulge (≈2 mag) and therefore it can be considered negligible from a dynamical standpoint, within our desired level of precision, thus simplifying significantly the analysis.

2.5 SPS masses

The photometry (typically in four bands, *BVIK*) is used to compute SPS masses using the method of Auger et al. (2009) together with Bruzual & Charlot (2003) SPS models. The SPS masses for the bulge and disc are computed using both Chabrier (2003) and Salpeter (1955) IMFs. We consider stellar populations described by five parameters: the total stellar mass $M_{\rm SPS}$, the population age A, the exponential star formation burst time-scale τ, the metallicity Z and the reddening due to dust, τ_V. We employ a uniform prior requiring $9 \leq \log_{10}(M_{\rm SPS}/{\rm M}_\odot) \leq 13$, the age is constrained such that star formation could begin at some (uniformly likely) time in the range $1 \leq z \leq 5$, τ has an exponential prior with characteristic scale 1 Gyr, and we impose uniform priors on the logarithms of the metallicity and dust extinction such that $-4 \leq \log_{10}Z \leq -1.3$ and $-2 \leq \log_{10}\tau_V \leq 0.3$. We note that the priors are the same for the bulge and the disc components but are sufficiently conservative that they do not bias our results. The posterior probability distribution function (PDF) is sampled as described in Auger et al. (2009). The stellar mass estimates are the mean and standard deviation of the marginalized posterior PDFs.

As discussed by several authors, especially for the old and mostly dust-free populations found in massive bulges, the uncertainties in stellar mass inferred from colours are dominated by the IMF normalization (see, e.g., recent discussion by Newman et al. 2012, and references therein). The degeneracies between ages and metallicities typical of colour-based inferences mostly cancel out when inferring stellar masses (Bell & de Jong 2001; Auger et al. 2009). Similarly, the effects of using different SPS models are typically of the order of 0.05–0.1 dex for stellar populations not dominated by thermally pulsating asymptotic giant branch stars (e.g. Treu et al. 2010).

3 REFERENCE MASS MODEL

In this section we define our reference model, which we will use in Section 4 to interpret the data. This is a very general model and should be regarded as the one providing the definitive results of this paper. However, in order to test the robustness of our conclusions, in Section 5 we define and apply to our data a full battery of alternative models, including ones with adiabatic contraction and expansion, as well as models characterized by dark matter cores, by different implementations of the cosmologically motivated dark matter haloes introduced here, and models without dark matter. As we will show, our conclusions are robust with respect to the choice of model. Therefore, the reader pressed for time can skip Section 5 and jump directly to Section 6 after Section 4.

3.1 Overview

Our reference model is one with two baryonic components, a spherical bulge and a thin disc, and a generic dark matter halo, that includes as a subset of standard profiles motivated by cosmological simulations. We refer to this model as the 'free' dark matter model.

We model the bulge with a Hernquist (1990) profile, which is parametrized by its mass, $M_{\rm bulge}$, and a half-mass radius, $r_{\rm bulge}$. We model the disc with an exponential profile, which is parametrized by its mass, $M_{\rm disc}$, and a half-mass radius $r_{\rm disc}$. We model the dark matter halo with a generalized spherical Navarro, Frenk & White (1997, NFW) profile:

$$\rho(r) \propto (r/r_{\rm s})^{-\gamma}(1 + r/r_{\rm s})^{-3+\gamma}, \tag{2}$$

where γ is the inner slope (NFW corresponds to $\gamma = 1$) and $r_{\rm s}$ is the scale radius. The normalization is determined by the virial velocity, V_{200}, which is defined at a radius, R_{200}, enclosing a mean density of 200 times the critical density of the Universe at redshift zero. The relation between virial velocity, virial radius and virial mass is thus given by

$$\frac{V_{200}}{({\rm km\,s^{-1}})} = \frac{R_{200}}{(h^{-1}\,{\rm kpc})} = \left(G\frac{M_{200}}{(h^{-1}\,{\rm M}_\odot)}\right)^{1/3}, \tag{3}$$

where $h = H_0/100\,{\rm km\,s^{-1}\,Mpc^{-1}}$ and $G \approx 4.302 \times 10^{-6}\,{\rm km^2\,s^{-2}\,kpc\,M_\odot}^{-1}$. This reference model thus has seven parameters (four for the baryons, three for the dark matter).

3.2 Constraints and priors

3.2.1 Baryons

The disc and bulge sizes are fixed to the values obtained from our photometric bulge–disc decompositions (from SWELLS I and III). This assumes negligible mass-to-light ratio gradients in the bulge and disc and leaves two free parameters, the masses of the bulge and the disc. For these we adopt uniform priors in $\log_{10}(M)$ over an interval bracketing the range of plausible values as inferred from SPS masses. In practice, we adopt a lower limit of half the SPS mass assuming a Chabrier IMF and an upper limit of twice the SPS mass assuming a Salpeter IMF. For old stellar populations, this upper limit corresponds to a power-law IMF with slope $\simeq -3$.

3.2.2 Dark matter

For the inner slope of the dark matter density profile we adopt a uniform prior in the interval $0 \leq \gamma < 2$. The lower limit corresponds to a cored halo, while the upper limit corresponds to isothermal, which mimics strong halo contraction.

For the scale radius of the halo we adopt a prior based on the concentration–mass relation of ΛCDM haloes from Macciò, Dutton & van den Bosch (2008). The median relation is given by

$$\log_{10}(c) = 0.830 - 0.098 \log_{10}\left(\frac{M_{200}}{10^{12}\,h^{-1}\,\mathrm{M}_{\odot}}\right). \quad (4)$$

The concentration, c, is defined to be the ratio between the virial radius and the radius where the slope of the density profile is -2: $c = R_{200}/r_{-2}$. For an NFW halo $r_{-2} = r_{\rm s}$, but for a generalized NFW halo $r_{-2} = r_{\rm s}/(2-\gamma)$. We adopt a Gaussian prior on $\log_{10}(c|M_{200})$ with a standard deviation of 0.11 dex, which is the scatter in halo concentrations found in cosmological simulations (Macciò et al. 2008). This choice of prior is not critical to our results. Its main purpose is to introduce more freedom in the dark matter model than obtained by assuming a fixed scale radius (e.g. Treu et al. 2010; Cappellari et al. 2012a) and to ensure that the scale radii are not unphysically large or small.

For the virial velocity of the dark matter halo we adopt a uniform prior in the interval $V_{200}^{\rm min} \leq V_{200} \leq V_{200}^{\rm max}\,\mathrm{km\,s^{-1}}$. The lower limit to the virial velocity is obtained by assuming that the baryon fraction (inside the virial radius) is equal to the cosmic baryon fraction, $f_{\rm bar} = 0.16$; thus,

$$V_{200}^{\rm min} = \left(\frac{G M_{\rm total}}{f_{\rm bar}/(1-f_{\rm bar})}\right)^{1/3} = \left(\frac{116.4}{\mathrm{km\,s^{-1}}}\right)\left(\frac{M_{\rm total}}{10^{11}\,\mathrm{M}_{\odot}}\right)^{1/3}, \quad (5)$$

where the total stellar mass $M_{\rm total} = M_{\rm bulge} + M_{\rm disc}$. Similarly, the upper limit $V_{200}^{\rm max}$ corresponds to a baryon-to-stars conversion efficiency of 1 per cent. This conservative limit is motivated by satellite kinematics, weak lensing and halo abundance matching, which find conversion efficiencies of $\gtrsim$2.5 per cent in massive galaxies (Dutton et al. 2010).

3.3 Mass model fitting

The model, parametrized by θ, is fitted to the kinematic and lensing data simultaneously using a Bayesian Markov chain Monte Carlo approach similar to that used in previous SWELLS papers. Specifically, we fit for the lensing Einstein radius b and the observed gas rotation curve $V_{\rm rot}(r_i)$ using the standard likelihood function

$$\mathcal{L}(\theta) = \exp\left\{-\frac{[b - b^{\rm mod}(\theta)]^2}{2\sigma_b^2} - \sum_i \frac{[V_{\rm rot}(r_i) - V_{\rm rot}^{\rm mod}(\theta)]^2}{2\sigma_{V,i}^2}\right\}. \quad (6)$$

As described above, our model for the gas rotation curve takes into account beam smearing due to seeing and finite slit width.

4 RESULTS

The results presented in this section are based on models with the 'free' dark matter halo described in Section 3. As discussed in Section 5, none of our main results are sensitive to the functional form of the dark matter halo that we adopt.

The results of our fits to the rotation curves and lensing Einstein radii are shown in the right-hand panels of Fig. 2. The black shaded region shows samples of acceptable models, which should be compared to the red and blue data points (which correspond to the receding and approaching sides of the rotation curve, respectively). The inset panels show the 1σ and 2σ constraints on the Einstein radius from strong lensing (SWELLS-III). The model Einstein radii are shown as histograms. The orange shaded regions show the 68 per cent confidence regions on the total circular velocity. The magenta, blue and grey shaded regions show the decomposition into bulge, disc and dark matter, respectively. Overall the models fit the data remarkably well and allow us to answer some specific questions.

4.1 Is the IMF universal within individual galaxies?

The posterior PDFs for the bulge and disc masses are shown in the left-hand panels of Fig. 2 next to the corresponding rotation curves. The marginalized constraints on the bulge, disc and total stellar masses are given in Table 2 (for reference, the corresponding masses from SPS models are given in Table 1). In the reference 'free' models, the disc stellar masses are somewhat loosely constrained due to the well-known disc–halo degeneracy (e.g. van Albada & Sancisi 1986). However, the bulge masses are well constrained because the inner part of the mass density profile is too steep to be described by the dark matter halo.

The grey circles in Fig. 2 correspond to a universal Chabrier IMF. Three of the five galaxies in our sample are inconsistent (at greater than the 2σ level) with a universal Chabrier IMF in *both* the bulge and disc. A heavier IMF is required for at least the bulge. Since Chabrier IMF seems to be in general preferred for star-forming galaxy discs, our data indicate that the IMF may be non-universal *within galaxies*.

A comparison between the bulge and disc masses from our lensing plus dynamics (LD) analysis, $M_{\rm LD}$, with those from SPS models, $M_{\rm SPS}$, is shown in Fig. 3. For the discs, the LD masses are consistent with a Chabrier IMF, in agreement with previous studies of galactic discs (e.g. Bell & de Jong 2001; Bershady et al. 2011; Dutton et al. 2011a; Barnabè et al. 2012). However for the bulges, the LD masses are a factor of $\simeq$2 higher than predicted by a Chabrier IMF and consistent with a Salpeter-like normalization. This latter result is in agreement with studies of massive ETGs (e.g. Auger et al. 2010; van Dokkum & Conroy 2010; Conroy & van Dokkum 2012; Dutton et al. 2012b; Spiniello et al. 2012). It is also interesting to note that the surface densities of the SWELLS bulges are comparable to the highest density ETGs in the local universe, which also favour IMFs with Salpeter-type normalization (Dutton et al. 2012a).

Fig. 4 shows the PDFs for the 'IMF mismatch parameter' Treu et al. (2010) $\alpha = M_{\rm LD}/M_{\rm SPS}$ quantifying the relation between LD masses and SPS masses. Uncertainties on both measurements are taken into account when deriving the posterior distribution of α. The mean and standard deviation of the PDFs from Fig. 4 are given in Table 2. On average, the IMF of bulges is a factor of $\sim$2 heavier than Chabrier ($\log\alpha_{\rm bulge} = 0.29 \pm 0.05$), while the IMF of the discs is consistent with Chabrier ($\log\alpha_{\rm disc} = -0.01 \pm 0.12$). We note that in four out of five galaxies the disc masses are also consistent with a Salpeter IMF. The total (bulge+disc) masses have $\log\alpha_{\rm total} = 0.24 \pm 0.04$, which is consistent with a Salpeter-like normalization of the IMF.

In SWELLS-III we concluded that a global IMF with α above the Salpeter value is ruled out (at 98 per cent confidence) for galaxies with lensing velocity dispersions below 230 km s^{-1}. This might seem at odds with the conclusions of this paper. However, three out of the five galaxies studied here have velocity dispersion greater than 230 km s^{-1} (see Table 1). The galaxies with higher velocity dispersions all favour bulge α values higher than the Salpeter value, while the galaxies with lower velocity dispersions favour bulge α values lower than the Salpeter value.

In addition, Table 2 gives the α parameter inside the Einstein radius calculated using results presented in SWELLS-III. Since

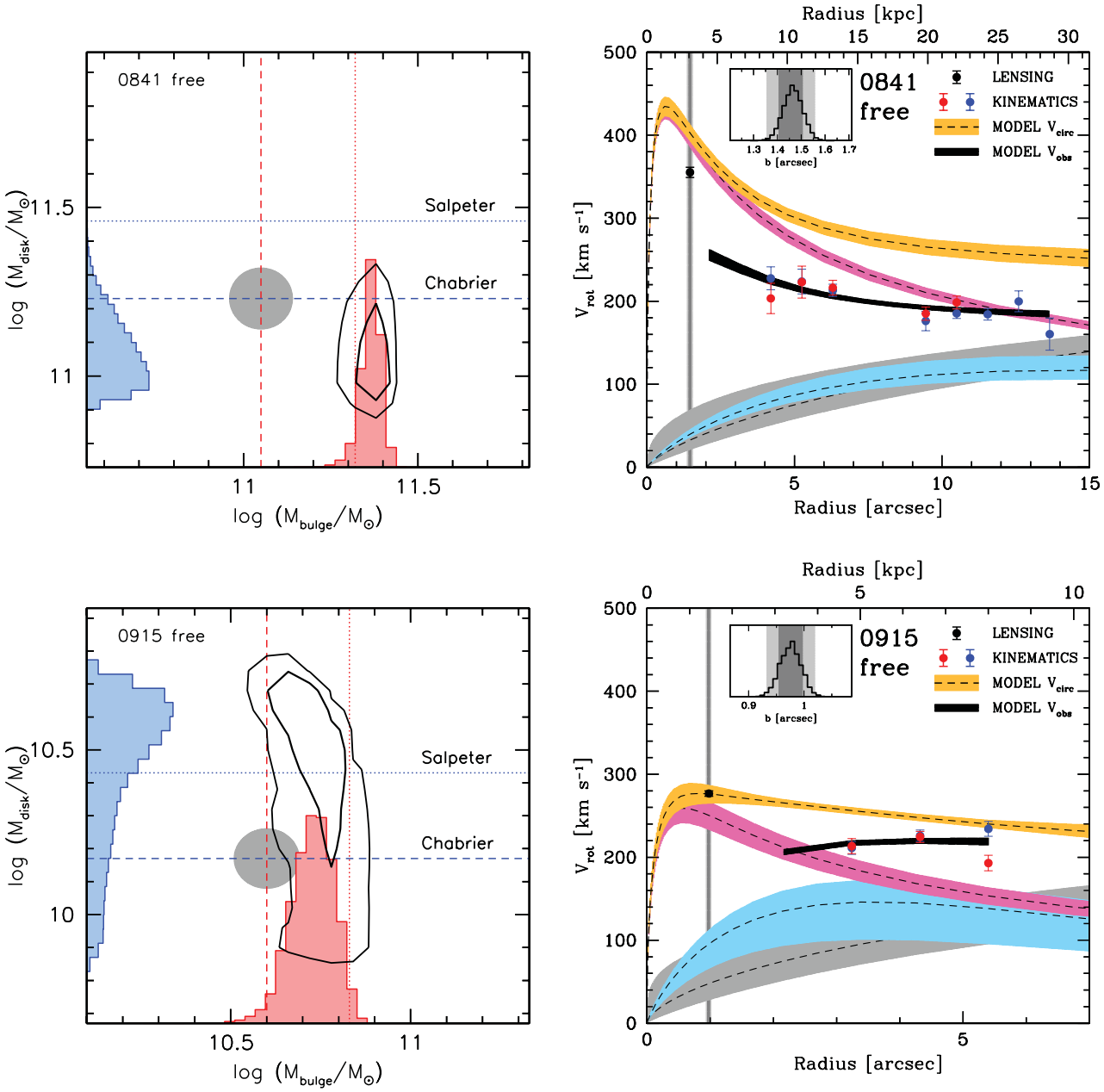

Figure 2. Mass model results for a free dark matter halo. Left: joint constraints on bulge and disc masses. The contours enclose 68 and 95 per cent of the probability. The red and blue histograms show the marginalized probability distributions for the bulge and disc masses, respectively. The dashed and dotted lines correspond to the median SPS masses assuming Chabrier and Salpeter IMFs, respectively. For reference, the grey ellipse shows the 1σ uncertainties on these SPS masses assuming a universal Chabrier IMF. Right: data model comparison. The black shaded region shows the 68 per cent confidence region of the 'observed' model (including inclination and beam smearing effects). This should be compared to the red and blue points, which correspond to the observed rotation velocities from the receding and approaching sides of the galaxy, respectively. In the inset panels, histograms show the distribution of model Einstein radii, while the shaded bands correspond to the 1σ and 2σ constraints on the observed Einstein radii. These grey bands are repeated in the main panel. For reference, the black point shows the circular velocity of the SIE model (note that this is not used in the fit). In the main panels, the orange shaded region shows the 68 per cent constraint on the total circular velocity profile. The magenta, cyan and grey shaded regions show the circular velocity profiles due to the bulge, disc and dark matter halo, respectively. The bulge masses are well constrained due to the declining nature of the circular velocity curves, while the disc masses are less well constrained, due to degeneracies with the dark matter halo.

these α are based on total masses, they are upper limits. Thus, for consistency they should be larger than the α we derive in this paper. A direct comparison is complicated because the α's are measured in different apertures, but nevertheless, the α values for the bulges that we derive here are fully consistent with the upper limits from SWELLS-III.

4.2 Are discs submaximal?

The rotation curves of spiral galaxies have contributions from the stellar mass, gas mass and dark matter. The relative contributions of each are difficult to estimate from rotation curve modelling due to well-known degeneracies. This led to the maximum disc hypothesis

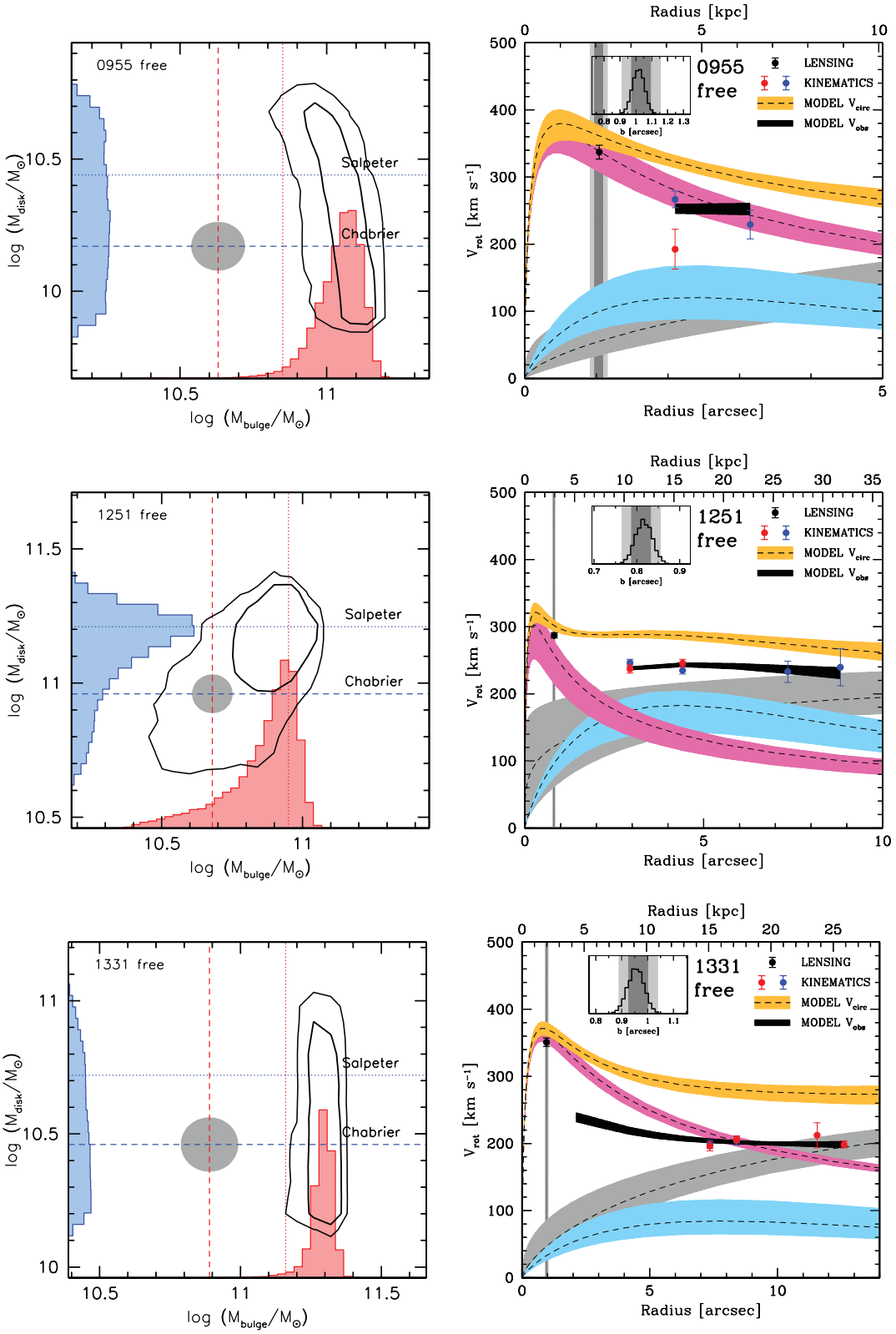

Figure 2 – *continued*

Table 2. Summary of stellar masses from fits to lensing and dynamics data with a free dark matter halo and a comparison with SPS-based masses. Columns 2, 3 and 4 give the stellar masses (median together with 68 per cent posterior probability) of the bulge, disc and total (bulge+disc); Columns 5, 6 and 7 give the IMF mismatch parameter $\alpha \equiv M_{\rm LD}/M_{\rm SPS}^{\rm Chab}$ (mean and standard deviation); Column 8 gives an upper limit to α within the Einstein radius using results directly from SWELLS-III.

Name (1)	$\log(M_{\rm LD,\,bulge})$ (2)	$\log(M_{\rm LD,\,disc})$ (3)	$\log(M_{\rm LD,\,total})$ (4)	$\log(\alpha_{\rm bulge})$ (5)	$\log(\alpha_{\rm disc})$ (6)	$\log(\alpha_{\rm total})$ (7)	$\log(\alpha_{\rm lens})$ (8)
J0841+3824	$11.37^{+0.02}_{-0.03}$	$11.06^{+0.12}_{-0.09}$	$11.54^{+0.05}_{-0.03}$	0.31 ± 0.10	-0.15 ± 0.13	0.10 ± 0.08	0.29 ± 0.10
J0915+4211	$10.73^{+0.06}_{-0.06}$	$10.50^{+0.14}_{-0.32}$	$10.94^{+0.03}_{-0.07}$	0.13 ± 0.11	0.27 ± 0.24	0.18 ± 0.09	0.09 ± 0.10
J0955+0101	$11.06^{+0.06}_{-0.08}$	$10.29^{+0.29}_{-0.27}$	$11.14^{+0.03}_{-0.05}$	0.41 ± 0.12	0.12 ± 0.26	0.37 ± 0.09	0.41 ± 0.08
J1251−0208	$10.90^{+0.07}_{-0.16}$	$11.16^{+0.10}_{-0.21}$	$11.35^{+0.07}_{-0.18}$	0.18 ± 0.15	0.15 ± 0.17	0.17 ± 0.14	0.33 ± 0.07
J1331+3638	$11.29^{+0.03}_{-0.04}$	$10.50^{+0.28}_{-0.23}$	$11.37^{+0.05}_{-0.04}$	0.40 ± 0.11	0.06 ± 0.25	0.34 ± 0.09	0.42 ± 0.09
Ensemble				0.29 ± 0.05	-0.01 ± 0.12	0.24 ± 0.04	

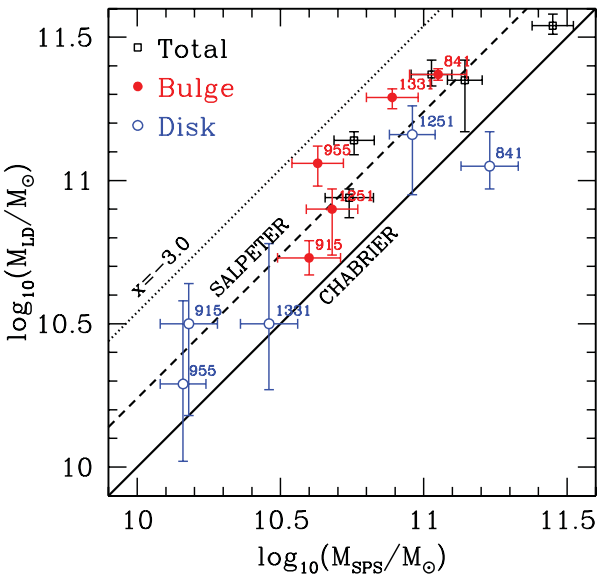

Figure 3. Comparison between bulge (red, filled circles), disc (blue, open circles) and total (black, squares) stellar masses from lensing plus dynamics, $M_{\rm LD}$, with those from SPS models assuming a Chabrier IMF, $M_{\rm SPS}$. The error bars enclose 68 per cent of the posterior probability. The disc masses of our five galaxies are consistent with a Chabrier IMF, but the bulge (and total) masses favour an IMF a factor of $\simeq 2$ heavier than Chabrier.

(e.g. van Albada & Sancisi 1986) which proposes that the stellar disc makes the maximum possible contribution to the rotation curve.

According to the standard definition (Sackett 1997), a disc is maximal if its contribution to the circular velocity at 2.2 disc scale lengths is $0.75 < V_{\rm disc}/V_{2.2} < 0.95$. This is shown as a blue shaded region in Fig.5. The blue circles in Fig. 5 show that our five galaxies have $V_{\rm disc}/V_{2.2} < 0.7$ and are thus submaximal. This is in broad agreement with results from the Disk Mass Project (solid and dashed lines in Fig. 5) which argued that all galaxy discs are submaximal (Bershady et al. 2011), in addition to earlier studies (e.g. Bottema 1993; Courteau & Rix 1999).

The galaxies in the Disk Mass Project are disc dominated, so submaximal discs imply that their galaxies are not baryon dominated inside 2.2 disc scale lengths (i.e. there is significant dark matter). However, in our galaxies there is a substantial bulge contribution (usually more than the disc) to $V_{2.2}$. The contribution of the stars (bulge plus disc) to $V_{2.2}$ is $\simeq 0.75$–0.95 (black points in Fig. 5), and thus these galaxies can be considered maximal in their total baryonic content at 2.2 disc scale lengths. (See also the results of the analysis of a disc galaxy lens including stellar kinematic constraints in SWELLS-IV; Barnabè et al. 2012.)

4.3 Are dark matter haloes cuspy?

The use of general dark matter haloes allows us to investigate the inner slope of the dark matter density profile, which is predicted by numerical simulations to be approximately unity, in the absence of baryons. Fig. 6 shows the PDFs of γ as inferred from our data. For individual galaxies γ is only weakly constrained, reflecting the fact that the bulge stellar mass dominates in the inner regions. Taken as an ensemble, and assuming a universal value for γ, values larger than unity (i.e. NFW) are marginally disfavoured [$p(\gamma > 1) = 0.07$], consistent with what is found for ETGs of comparable mass (Treu & Koopmans 2004; Dutton et al. 2012b), albeit there are counterexamples (Grillo 2012; Sonnenfeld et al. 2012), which may indicate that there is a broad scatter stemming perhaps from different formation histories.

At face value this result would imply a marginal conflict with the universal profiles predicted by CDM only numerical simulations. However, since the central regions of these galaxies are baryon dominated, an accurate comparison depends crucially on how baryonic effects alter the underlying dark matter haloes. Standard arguments suggest that baryonic cooling to form stars should steepen the overall mass density profile, thus causing the dark matter halo to steepen as well (Blumenthal et al. 1986; Gnedin et al. 2004). This would only exacerbate the tension between our observations and theoretical prediction. However, in practice other processes may occur that act to expand the halo, such as mass outflows due to stellar and/or active galactic nuclei (e.g. Read & Gilmore 2005; Duffy et al. 2010; Pontzen & Governato 2012) or dynamical friction between infalling galaxies and the dark matter haloes (e.g. El-Zant, Shlosman & Hoffman 2001; Johansson et al. 2009). Investigating this complex physics in detail goes beyond the scope of this paper, but it is interesting to note that our data suggest that the net effect of baryonic physics appears to lead to real haloes that are flatter or at most as flat as NFW, and not as cuspy as the standard contraction recipes would imply.

5 TESTING SYSTEMATIC EFFECTS

In this section we discuss how our results depend on the functional form of the dark matter halo (Section 5.1), and we test potential systematic uncertainties arising from contamination of the lensing signal by mass along the line of sight (Section 5.2). In Section 5.3 we discuss briefly the effects of neglecting cold gas in our lensing

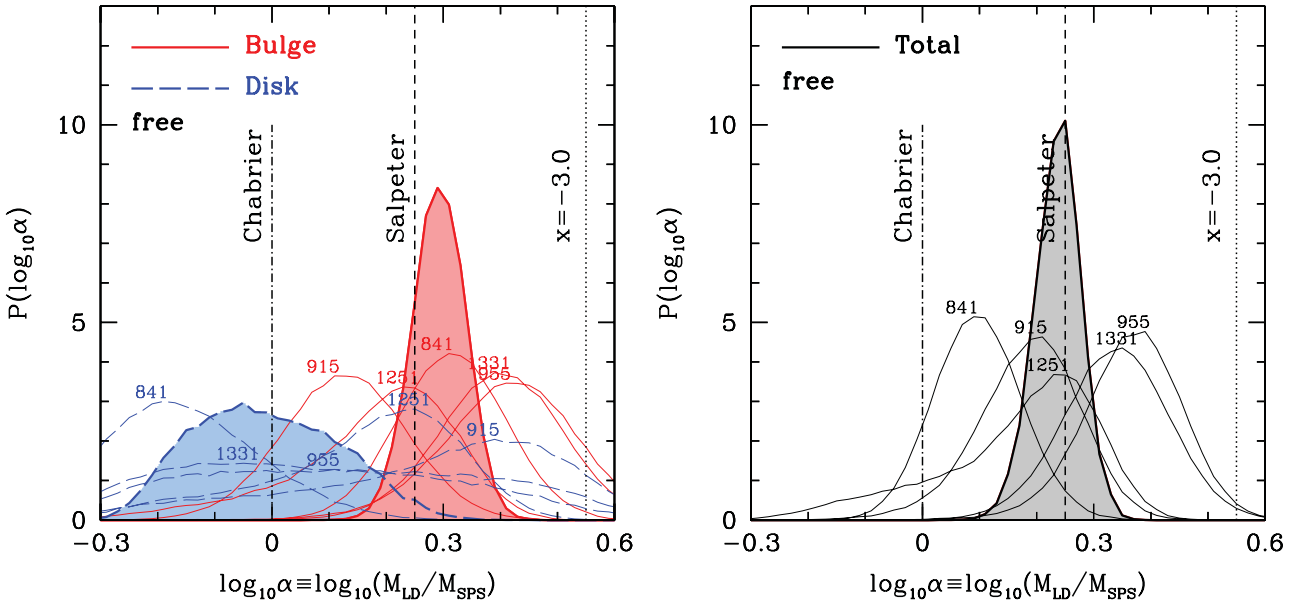

Figure 4. Posterior distributions for the IMF mismatch parameter relative to a Chabrier IMF, α. Left: for bulges (red, solid lines) and discs (blue, long dashed lines); Right: for total (bulge+disc) stellar mass. The bold histograms show the joint constraints on the mean α. Discs are consistent with a Chabrier IMF, while bulges require an IMF roughly twice as heavy as a Chabrier IMF. The overall normalization is close to Salpeter.

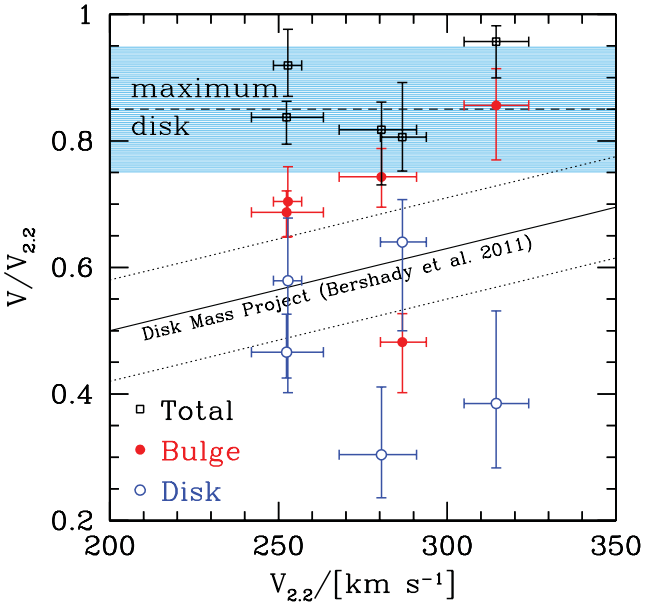

Figure 5. Contribution of disc, bulge and bulge+disc to circular velocity at 2.2 disc scale lengths. Discs are submaximal in agreement with the Disk Mass Project (Bershady et al. 2011), where the solid and dashed lines correspond to their best-fitting relation and scatter, respectively. However, the contribution of the disc plus bulge at 2.2 disc scale lengths is maximal, and thus our galaxies are baryon dominated within 2.2 disc scale lengths.

and dynamical analysis. We find that our conclusions are robust with respect to the choice of mass models and line-of-sight effects, and the inclusion of cold gas.

5.1 Alternative dark matter halo models

Our inferred dark matter profile is less cuspy than the NFW profile and one may be concerned that we have fitted away part of the central dark matter into our bulge component, thus leading to the preference for Salpeter-like IMFs over Chabrier. We therefore also consider a wide range of less flexible dark matter haloes, ranging from models with no dark matter or 'mass-follows-light' ('mfl'), to cored dark matter haloes ('core'), to contracted NFW haloes ('ac', 'weakac' and 'freeac'). The most generic model adopted by the ATLAS3D team in their recent study (Cappellari et al. 2012a) is also included to facilitate comparisons between our works ('atlas').

The contracted NFW haloes are meant to represent the response of the dark matter halo to galaxy formation. The simple model 'ac' refers to the standard Blumenthal et al. (1986) formalism, the 'weakac' model is the reduced contraction model of Abadi et al. (2010), while the 'freeac' model is a generalization. In the standard formalism, the adiabatic invariant is $rM(r)$, where r is the galactic radius and $M(r)$ is the spherically enclosed mass within r. Thus,

$$r_{\rm f}/r_{\rm i} = M_{\rm i}(r_{\rm i})/M_{\rm f}(r_{\rm f}), \qquad (7)$$

where $r_{\rm i}$ and $r_{\rm f}$ are the initial and final radii, respectively.

In order to explore the possibility of weaker halo contraction (e.g. Abadi et al. 2010) and even expansion, we also consider the generalized contraction formula from Dutton et al. (2007). If the standard contraction ratio from equation (7) is $\Gamma = (r_{\rm f}/r_{\rm i})$, then the modified contraction ratio is given by Γ^{ν}. Standard adiabatic contraction (Blumenthal et al. 1986) corresponds to $\nu = 1$, the Gnedin et al. (2004) model can be approximated with $\nu \sim 0.8$ and the Abadi et al. (2010) model can be approximated with $\nu \sim 0.4$; no contraction corresponds to $\nu = 0$, while expansion corresponds to $\nu < 0$.

Table 3 lists the dark halo priors for the eight models we consider here. We note that the models 'core' and 'nfw' are specific realizations of the model 'free', and the models 'ac' and 'nfw' are specific realizations of the model 'freeac'.

The posterior PDFs for the IMF mismatch parameters of the bulge, disc and total stellar mass for all models (our reference 'free' model and alternatives) are given in Fig. 7. As expected, the disc masses are somewhat sensitive to the choice of dark matter halo. However, the bulge masses are remarkably insensitive to

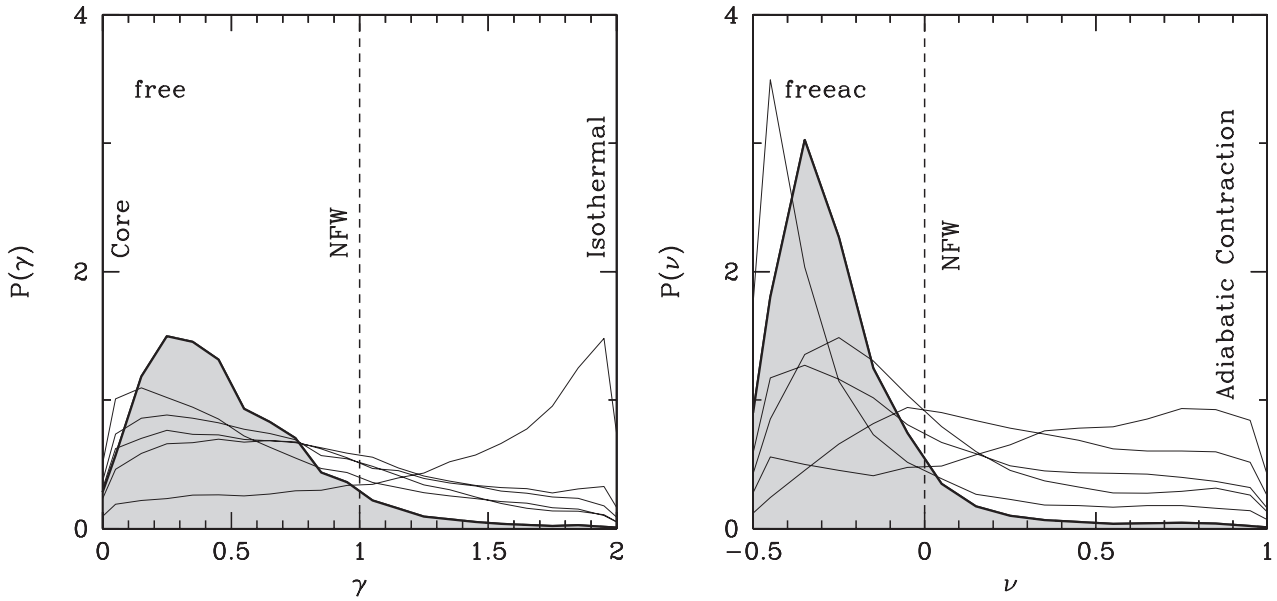

Figure 6. Posterior distributions for the central slope of the dark matter density profile, γ (left-hand panel), and halo response parameter, ν (right-hand panel). The bold histograms show the joint constraint on the mean. Haloes with $\gamma \gtrsim 1$ or halo contraction $\nu > 0$ are, on average, disfavoured.

Table 3. Summary of priors on dark matter halo for our various mass models. $U(a, b)$ is a uniform prior with limits a and b. $\delta(a)$ is a delta function prior at a.

Model	γ	ν	r_s	V_{200}
free	$U(0.0, 2.0)$	$\delta(0.0)$	$r_s(V_{200})$	$U(V_{200}^{min}, V_{200}^{max})$
atlas	$U(0.0, 1.6)$	$\delta(0.0)$	$\delta(20\,\mathrm{kpc})$	$U(V_{200}^{min}, V_{200}^{max})$
mfl	–	–	–	–
core	$\delta(0.0)$	$\delta(0.0)$	$r_s(V_{200})$	$U(V_{200}^{min}, V_{200}^{max})$
nfw	$\delta(1.0)$	$\delta(0.0)$	$r_s(V_{200})$	$U(V_{200}^{min}, V_{200}^{max})$
weakac	$\delta(1.0)$	See the text	$r_s(V_{200})$	$U(V_{200}^{min}, V_{200}^{max})$
ac	$\delta(1.0)$	$\delta(1.0)$	$r_s(V_{200})$	$U(V_{200}^{min}, V_{200}^{max})$
freeac	$\delta(1.0)$	$U(-0.5, 1.0)$	$r_s(V_{200})$	$U(V_{200}^{min}, V_{200}^{max})$

the dark matter halo model. All of the models, with the exception of adiabatically contracted NFW haloes (model 'ac'), favour Salpeter-type IMFs for the bulges. The 'ac' model is the only one that favours Chabrier-type IMFs for the bulges. However, the fact that the 'freeac' model contains the 'ac' model allows us to perform a clean model selection procedure and quantify whether the models with Salpeter IMF or the 'ac' model provides a better overall description of the data. Qualitatively, as can be seen from Fig. 6, the 'freeac' model prefers values of the contraction index that disfavour the standard adiabatic contraction models. Quantitatively, the comparison between the 'freeac' model and the 'ac' model is given by the evidence ratio (Sivia & Skilling 2006). The evidence of the 'freeac' model is 35 times larger than that of the 'ac' model, which further corresponds to strong evidence that the first model is to be preferred according to standard criteria (Sivia & Skilling 2006). Similar considerations can be made for the IMF mismatch parameter α of the discs, although in general it is less well constrained than that of the bulge. All models with dark matter prefer discs that are Chabrier or lighter, except for the 'nfw' and 'core' models. Those are subsets of the 'free' model and are disfavoured by the evidence ratios.

We thus conclude that *it is possible* to reconcile the data with a Chabrier IMF for bulges if one asserts that standard adiabatic contraction is the way dark matter haloes respond to galaxy formation. However, cosmological simulations of galaxy formation often find much weaker contraction than predicted by the adiabatic contraction formalism (Johansson et al. 2009; Abadi et al. 2010; Tissera et al. 2010) or even expansion (Governato et al. 2010; Macciò et al. 2012), and thus we do not actually expect adiabatic contraction to occur in nature. Furthermore, under the more general assumption of ignorance about the effects of galaxy formation on the underlying dark matter halo, the data clearly prefer uncontracted or mildly expanded haloes with a Salpeter IMF. This is true for a broad range of models, including our 'free' models, our 'freeac' models and the 'atlas' models.

5.2 Line-of-sight effects

Another potential concern is whether excess mass along the line of sight could lead us to overestimate the mass associated with the main deflector and thus overestimate α. This is usually described in the lensing literature as external convergence (κ_{ext}; e.g. Suyu et al. 2010; Treu et al. 2010). The excess/deficit mass along the line of sight acts to first approximation as a sheet of mass at the redshift of the deflector, expressed in units of the critical density κ_{crit}, and cannot be measured with pure lensing arguments due to the well-known mass sheet degeneracy (Falco, Gorenstein & Shapiro 1985). External convergence affects the lensing observable used in our analysis – the amount of mass within the Einstein radius – in a very simple manner. The true mass will just be the observed mass obtained by assuming that the line of sight has the average density of the universe, multiplied by $(1-\kappa_{ext})$, for small values of κ_{ext}.

At the relatively low redshift of the SWELLS and SLACS samples, external convergence is very small. Detailed analysis of the SLACS sample shows that the external convergence is typically a few per cent (e.g. Treu et al. 2009; Guimarães & Sodré 2011; Sonnenfeld et al. 2012). Thus, we expect that external convergence will change our results by a few per cent at most. For completeness,

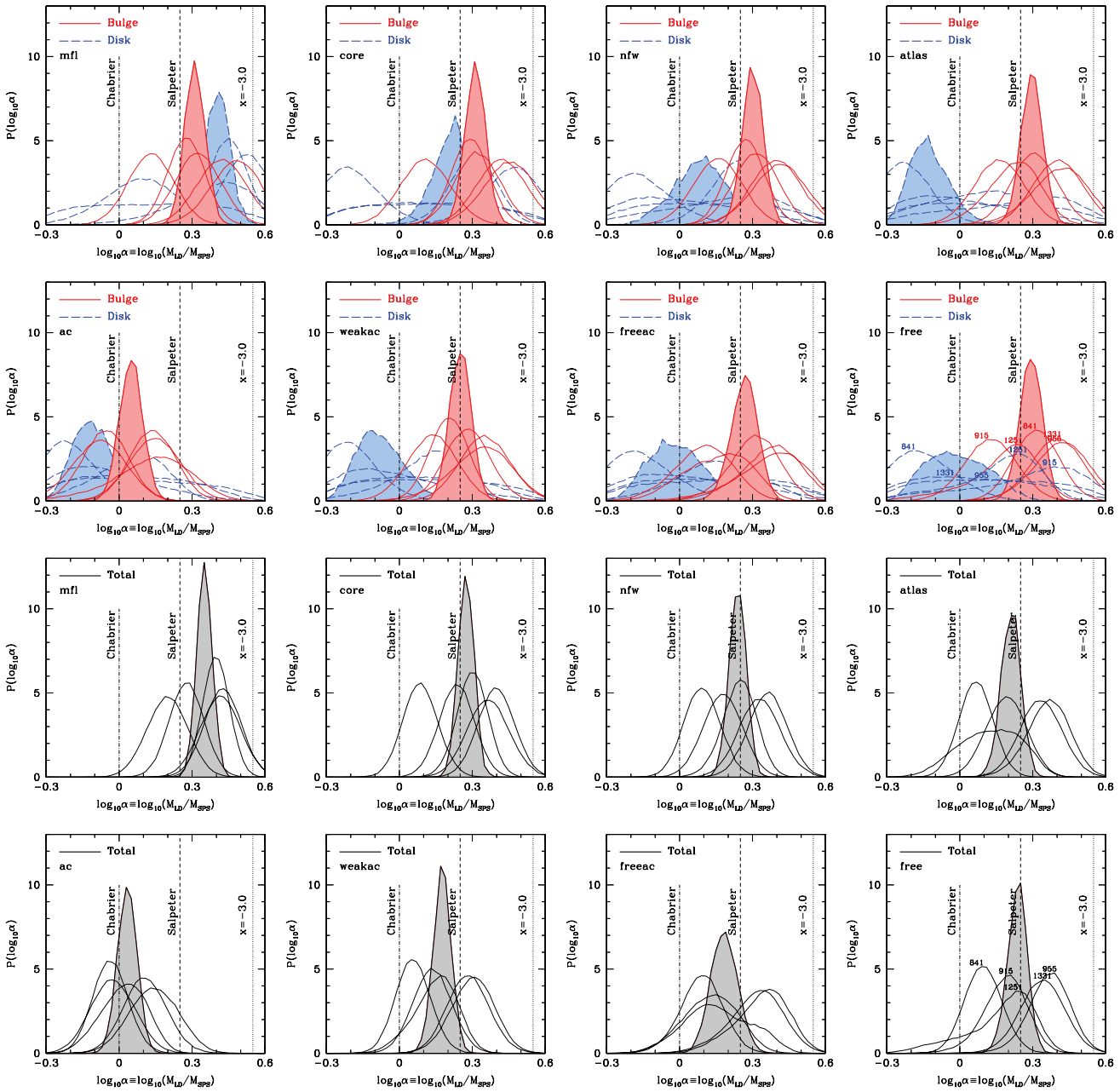

Figure 7. Posterior distributions for the IMF mismatch parameter relative to a Chabrier IMF, α, for eight different assumptions about the functional form of the dark matter halo: mfl – mass-follows-light (i.e. no dark matter halo); core – cored dark matter halo; nfw – Navarro et al. (1997) dark matter halo, constrained to follow the concentration–mass relation from Macciò et al. (2008) allowing for scatter; ac – adiabatically contracted nfw model; weakac – nfw model with weak halo contraction following Abadi et al. (2010); freeac – nfw model with free halo response ranging from adiabatic contraction to expansion; atlas – halo profile adopted by ATLAS3D (Cappellari et al. 2012a) which is a generalized NFW with fixed scale radius; free – generalized NFW halo with free inner slope (repeated from Fig. 4). Upper: α for bulges (red, solid lines) and discs (blue, long dashed lines); Lower: α for total (bulge+disc) stellar mass. The bold histograms show the joint constraints on the mean α. For all models except 'ac', the bulges are consistent with a Salpeter IMF. For 'ac', the bulges are consistent with a Chabrier IMF, but allowing the halo response to vary 'freeac' generally finds better fits with weaker halo contraction or expansion.

we repeated all our inference assuming $\kappa_{\rm ext} = 0.05$. As expected, α shifts down by a negligible amount (compare models 'free' to 'free+$\kappa_{\rm ext}$' in Fig. 8) demonstrating that our inferences are robust with respect to line-of-sight effects.

5.3 Cold gas

In principle, the stellar masses derived from our lensing plus dynamics fits are upper limits, because we do not include cold gas in our mass models. For the stellar masses of our galaxies we expect cold gas fractions of $\sim$20 $\pm$ 10 per cent (e.g. Dutton et al. 2011a), roughly equally split between atomic and molecular gas. Molecular gas generally traces the stars and is typically less than $\sim$10 per cent of the stellar mass, assuming a Chabrier IMF (Saintonge et al. 2011), so the effect on our derived bulge stellar masses is expected to be less than 0.05 dex. The atomic gas typically has a larger scale length than the stellar disc, so we expect the atomic gas to subtract mass from the stellar disc and dark matter halo. In summary, we

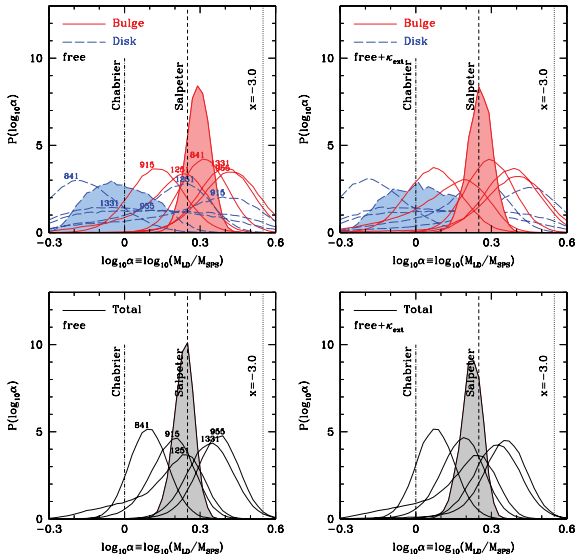

Figure 8. Effect of external convergence on the posterior distributions for the IMF mismatch parameter relative to a Chabrier IMF, α, for the 'free' model. The model 'free+$\kappa_{\rm ext}$' (right-hand panels) has the same dark matter halo as 'free' (left-hand panels, repeated from Fig. 4), except that we have included 5 per cent external convergence. The effect of external convergence is to lower α by a small amount.

expect that including observations of cold gas in our mass models will not significantly reduce the derived stellar masses of the bulges.

6 SUMMARY

We have presented mass models of five massive galaxies selected from the SWELLS survey (Treu et al. 2011) to have bulges and discs of comparable stellar mass, as well as star-forming discs. We combined masses from strong lensing with ionized gas kinematics at ∼1–3 disc scale lengths to constrain the parameters of three-component mass models consisting of a bulge, a disc and a generic dark matter halo. Our main results can be summarized as follows.

(i) The stellar masses of the bulges are well constrained by the lensing and kinematic data, independent of the inner density slope of the dark matter halo.

(ii) The bulge masses inferred from the lensing and dynamical models, $M_{\rm LD}$, are inconsistent with those obtained from the colours, $M_{\rm SPS}$, assuming a Chabrier IMF, but in good agreement with those based on a Salpeter IMF. The average normalization of the IMF of the bulges relative to that based on a Chabrier IMF is given by the IMF mismatch parameter $\log_{10}\alpha_{\rm bulge} \equiv \log_{10}(M_{\rm LD,bulge}/M^{\rm Chab}_{\rm SPS,bulge}) = 0.29 \pm 0.05$

(iii) The disc masses inferred from the lensing and dynamical models are only weakly constrained, due to degeneracies with the dark matter halo, but are consistent with a Chabrier-like IMF. The average IMF mismatch parameter is found to be $\log_{10}\alpha_{\rm disc} = -0.01 \pm 0.12$.

(iv) Discs are submaximal at 2.2 disc scale lengths (in agreement with the Disk Mass Project; Bershady et al. 2011). However, baryons dominate the potential inside 2.2 disc scale lengths due to the strong bulge components. And thus submaximal discs do not imply that galaxies are dark matter dominated inside 2.2 disc scale lengths.

(v) The data marginally disfavour an inner slope of the dark matter halo of $\gamma > 1$ that would be expected for NFW haloes contracted according to standard adiabatic contraction prescriptions. Equivalently, the data favour an uncontracted or marginally expanded NFW halo.

Our main new result is that IMF of bulges of spirals is 'heavier' than Chabrier, and consistent with a Salpeter IMF. Since our data do not strongly constrain the IMF of the discs, there are two possible implications. Either the IMF varies *between* spiral galaxies (e.g. massive spiral galaxies have heavier IMFs than the Milky Way) or the IMF varies *within* spiral galaxies (e.g. bulges have heavier IMFs than discs). Since all previous constraints on the masses of galactic discs seem to rule out Salpeter IMFs (e.g. Bell & de Jong 2001; Bershady et al. 2011; Dutton et al. 2011a; Martinsson 2011; Barnabè et al. 2012), we favour the latter hypothesis. Even though this result might seem surprising, it is well known that the stellar populations of bulges and discs differ in age and chemical composition. Thus, if the IMF reflects the physical conditions at the time of formation of the stellar populations, it is entirely possible that it could be different for the bulge and disc. Clearly, even though this is possible, the underlying physical reasons are at present unclear. Our hope is that this new piece of the puzzle will be a valuable clue for deciphering the mystery of the IMF and its variations across the universe.

To conclude we note that our results are consistent with previous work based on completely different techniques and samples when reframed in terms of a global IMF (as summarized by, e.g., Treu et al. 2010; Cappellari et al. 2012b). Furthermore, our hypothesis of a different IMF for bulge and disc is consistent with the upper limits on the total mass within the Einstein radius for the entire SWELLS and SLACS samples, presented in a companion paper (Brewer et al., in preparation). Whereas SWELLS-III showed that the SWELLS and SLACS data are consistent with an IMF that changes as a function of galaxy stellar mass of stellar velocity dispersion, Brewer et al. (in preparation) show that a scenario where the IMF is Salpeter-like in the bulge and Chabrier-like in the disc is perfectly consistent with the lensing constraints.

ACKNOWLEDGMENTS

AAD acknowledges financial support from the National Science Foundation Science and Technology Center CfAO, managed by UC Santa Cruz under cooperative agreement No. AST-9876783. AAD was partially supported by HST grants GO-12292, GO-11978 and GO-11202. TT acknowledges support from the NSF through CAREER award NSF-0642621, and from the Packard Foundation through a Packard Research Fellowship. PJM was given support by the Royal Society in the form of a research fellowship. MB acknowledges support from the Department of Energy contract DE-AC02-76SF00515. DCK acknowledges support from HST grant GO-11206.02-A, and NSF grant AST-0808133. LVEK acknowledges the support by an NWO-VIDI programme subsidy (programme number 639.042.505). This research is supported by NASA through *Hubble Space Telescope* programmes GO-10587, GO-10886, GO-10174, 10494, 10798, 11202, 11978 and 12292, and in part by the National Science Foundation under Grant No. PHY99-07949 and is based on observations made with the NASA/ESA *Hubble Space Telescope* and obtained at the Space Telescope Science Institute, which is operated by the Association of Universities for Research in Astronomy, Inc., under NASA contract NAS 5-26555, and at the W.M. Keck Observatory, which is operated as a scientific partnership among the California Institute of Technology, the University of California and the National Aeronautics and Space Administration. The Observatory was made possible by the generous financial support of the W.M. Keck Foundation. The authors

wish to recognize and acknowledge the very significant cultural role and reverence that the summit of Mauna Kea has always had within the indigenous Hawaiian community. We are most fortunate to have the opportunity to conduct observations from this mountain. Funding for the SDSS and SDSS-II was provided by the Alfred P. Sloan Foundation, the Participating Institutions, the National Science Foundation, the US Department of Energy, the National Aeronautics and Space Administration, the Japanese Monbukagakusho, the Max Planck Society, and the Higher Education Funding Council for England. The SDSS was managed by the Astrophysical Research Consortium for the Participating Institutions. The SDSS website is http://www.sdss.org/.

REFERENCES

Abadi M. G., Navarro J. F., Fardal M., Babul A., Steinmetz M., 2010, MNRAS, 407, 435
Amorisco N. C., Bertin G., 2010, A&A, 519, A47
Auger M. W., Treu T., Bolton A. S., Gavazzi R., Koopmans L. V. E., Marshall P. J., Bundy K., Moustakas L. A., 2009, ApJ, 705, 1099
Auger M. W., Treu T., Gavazzi R., Bolton A. S., Koopmans L. V. E., Marshall P. J., 2010, ApJ, 721, L163
Barnabè M. et al., 2012, MNRAS, 423, 1073
Bastian N., Covey K. R., Meyer M. R., 2010, ARA&A, 48, 339
Bell E. F., de Jong R. S., 2001, ApJ, 550, 212
Bershady M. A., Martinsson T. P. K., Verheijen M. A. W., Westfall K. B., Andersen D. R., Swaters R. A., 2011, ApJ, 739, L47
Bertin G. et al., 1994, A&A, 292, 381
Blanton M. R., Moustakas J., 2009, ARA&A, 47, 159
Blumenthal G. R., Faber S. M., Flores R., Primack J. R., 1986, ApJ, 301, 27
Bottema R., 1993, A&A, 275, 16
Brewer B. J. et al., 2012, MNRAS, 422, 3574
Bruzual G., Charlot S., 2003, MNRAS, 344, 1000
Cappellari M. et al., 2006, MNRAS, 366, 1126
Cappellari M. et al., 2012a, Nat, 484, 485
Cappellari M. et al., 2012b, arXiv:1208.3523
Chabrier G., 2003, PASP, 115, 763
Conroy C., van Dokkum P., 2012, arXiv:1205.6473
Courteau S., Rix H.-W., 1999, ApJ, 513, 561
Duffy A. R., Schaye J., Kay S. T., Dalla Vecchia C., Battye R. A., Booth C. M., 2010, MNRAS, 405, 2161
Dutton A. A., Courteau S., de Jong R., Carignan C., 2005, ApJ, 619, 218
Dutton A. A., van den Bosch F. C., Dekel A., Courteau S., 2007, ApJ, 654, 27
Dutton A. A., Conroy C., van den Bosch F. C., Prada F., More S., 2010, MNRAS, 407, 2
Dutton A. A. et al., 2011a, MNRAS, 416, 322
Dutton A. A. et al., 2011b, MNRAS, 417, 1621
Dutton A. A., Mendel J. T., Simard L., 2012a, MNRAS, 422, L33
Dutton A. A., Maccio A. V., Mendel J. T., Simard L., 2012b, arXiv:1204.2825
El-Zant A., Shlosman I., Hoffman Y., 2001, ApJ, 560, 636
Falco E. E., Gorenstein M. V., Shapiro I. I., 1985, ApJ, 289, L1
Gnedin O. Y., Kravtsov A. V., Klypin A. A., Nagai D., 2004, ApJ, 616, 16
Governato F. et al., 2010, Nat, 463, 203
Grillo C., 2012, ApJ, 747, L15
Guimarães A. C. C., Sodré L. Jr, 2011, ApJ, 728, 33
Hall M., Courteau S., Dutton A. A., McDonald M., Zhu Y., 2012, MNRAS, 425, 2741
Hernquist L., 1990, ApJ, 356, 359
Johansson P. H., Naab T., Ostriker J. P., 2009, ApJ, 697, L38
Koopmans L. V. E., Treu T., 2003, ApJ, 583, 606
Kroupa P., 2001, MNRAS, 322, 231
Macciò A. V., Dutton A. A., van den Bosch F. C., 2008, MNRAS, 391, 1940
Macciò A. V, Stinson G, Brook C. B., Wadsley J., Couchman H. M. P., Shen S., Gibson B. K., Quinn T., 2012, ApJ, 744, L9
Martinsson T. P. K., 2011, PhD thesis, Univ. Groningen
McKee C. F., Ostriker E. C., 2007, ARA&A, 45, 565
Navarro J. F., Frenk C. S., White S. D. M., 1997, ApJ, 490, 493
Newman A. B., Treu T., Ellis R. S., Sand D. J., 2012, arXiv:1209.1392
Oke J. B. et al., 1995, PASP, 107, 375
Pontzen A., Governato F., 2012, MNRAS, 421, 3464
Read J. I., Gilmore G., 2005, MNRAS, 356, 107
Sackett P. D., 1997, ApJ, 483, 103
Saintonge A. et al., 2011, MNRAS, 415, 32
Salpeter E. E., 1955, ApJ, 121, 161
Sivia D. S., Skilling J., 2006, Data Analysis: A Bayesian Tutorial, 2nd edn. Oxford Univ. Press, Oxford
Sonnenfeld A., Treu T., Gavazzi R., Marshall P. J., Auger M. W., Suyu S. H., Koopmans L. V. E., Bolton A. S., 2012, ApJ, 752, 163
Spiniello C., Koopmans L. V. E., Trager S. C., Czoske O., Treu T., 2011, MNRAS, 417, 3000
Spiniello C., Trager S. C., Koopmans L. V. E., Chen Y., 2012, ApJ, 753, L32
Suyu S. H., Marshall P. J., Auger M. W., Hilbert S., Blandford R. D., Koopmans L. V. E., Fassnacht C. D., Treu T., 2010, ApJ, 711, 201
Tissera P. B., White S. D. M., Pedrosa S., Scannapieco C., 2010, MNRAS, 406, 922
Treu T., 2010, ARA&A, 48, 87
Treu T., Koopmans L. V. E., 2002, ApJ, 575, 87
Treu T., Koopmans L. V. E., 2004, ApJ, 611, 739
Treu T., Gavazzi R., Gorecki A., Marshall P. J., Koopmans L. V. E., Bolton A. S., Moustakas L. A., Burles S., 2009, ApJ, 690, 670
Treu T., Auger M. W., Koopmans L. V. E., Gavazzi R., Marshall P. J., Bolton A. S., 2010, ApJ, 709, 1195
Treu T., Dutton A. A., Auger M. W., Marshall P. J., Bolton A. S., Brewer B. J., Koo D. C., Koopmans L. V. E., 2011, MNRAS, 417, 1601
van Albada T. S., Sancisi R., 1986, R. Soc. Lond. Philos. Trans. Series A, 320, 447
van Dokkum P. G., Conroy C., 2010, Nat, 468, 940
van Dokkum P. G., Conroy C., 2011, ApJ, 735, L13
Wyse R. F. G., Gilmore G., Franx M., 1997, ARA&A, 35, 637

This paper has been typeset from a TEX/LATEX file prepared by the author.